Journal of The Electrochemical Society, **153** (3) A607-A613 (2006)
0013-4651/2006/153(3)/A607/7/$20.00 © The Electrochemical Society

Lattice Boltzmann Simulation on Molten Carbonate Fuel Cell Performance

Y. S. Xu,[a,b,c,z] Y. Liu,[b] X. Z. Xu,[d] and G. X. Huang[a]

[a]*Department of Physics, East China Normal University, Shanghai 200062, China*
[b]*Department of Mechanical Engineering, The Hong Kong Polytechnic University, Kowloon, Hong Kong, China*
[c]*Department of Physics, Zhejiang Normal University, Jinhua 321004, China*
[d]*Department of Mechanics and Mechanical Engineering, University of Science and Technology of China, Hefei 230027, China*

Based on a model of a porous electrode, we make a detailed numerical simulation on molten carbonate fuel cell (MCFC) performance by using the lattice Boltzmann method (LBM). We apply Brinkman-Forchheimer-extended Darcy equations (generalized momentum equation) together with a reaction-diffusion equation with several reasonable assumptions and, to simulate more realistic physical conditions, we consider a curved boundary lying between the nodes of equal lattice space. As an attempt to assess the validity and efficiency of our model, two benchmark problems are investigated, including (*i*) the calculation of the dependence of generated current density on averaged gas velocity and the comparison between the result obtained by the LBM and by some other analytical solutions; (*ii*) the comparison between the result by the LBM calculation and the one by measuring experimentally the current density of test series in an overall range of H_2 concentration. An excellent agreement is found between the results from the LBM calculation and those from the experiment. In addition, the dependence of CO_2 removal rate on current density, the contributions of CO_2 concentration and O_2 concentration on cell performance, and the relations of cell voltage and power density with current density (load) are also studied.
 [DOI: 10.1149/1.2164807]

Manuscript submitted August 30, 2005; revised manuscript received November 28, 2005.
Available electronically February 1, 2006.

The molten carbonate fuel cell (MCFC) is an electrochemical power generator with potential applications for attaining very high electrical energy conversion efficiency while operating quietly with minimal polluting emissions. In such a cell, the cathode is NiO, the anode is Ni, and the electrolyte is a carbonate compound of alkaline metals (Li_2CO_3, K_2CO_3, etc.). Efficiency ranges from 60 to 80%, and operating temperature is about 650°C. Units with output up to 2 MW have been constructed, and designs exist for units up to 100 MW. Considerable research and development of MCFC have been carried out mainly in the United States, Japan, and Europe. A successful application of MCFC requires accurate prediction of unit-cell performance and operation characteristics. Generally, MCFC operation can be characterized as fluid transport and transformation of species by an electrochemical reaction. Numerical computation is used to realize the quantizing prediction, emulation, and analysis of MCFC performance under a large range of operation and different transient conditions.

Usually, numerical models for MCFC can be categorized into two classes: microscopic (porous-electrode models) and macroscopic (cell-performance models).[1,2] In this work, we focus on porous-electrode model. Note that two well-known porous-electrode models have been derived for MCFC. They are the thin-film model[3] and the agglomerate model.[4] Fontes et al.[5] presented a steady-state agglomerate model for a MCFC cathode, which takes into account the heterogeneous structure of a porous electrode. In their approach, the resulting model equations were solved by means of a finite-element method, but their simulation results were limited to a small agglomerate. Two years later, Fontes and co-workers[6] analyzed experimental polarization curves by means of numerical modeling and obtained, under more specific conditions, approximated linear polarization curves for MCFC. Fehribach et al.[7] obtained a numerical model for the peroxide mechanism on electrochemistry of MCFC. Their model has several advantages, including an elegant combination of chemical and electrical processes, a clear connection to the underlying reaction stoichiometry, and the fewest equations required to be consistent with stoichiometry. Subramanian[8] developed a numerical model by using a three-phase homogeneous approach. The model indicates that the mass transfer effect becomes important at a high current density. Mangold and Sheng[9] established a reduced nonlinear numerical model with internal reforming. Fermeglia et al.[10] established a model for steady-state-process simulation, and Yoshiba[11] established a thermal model. Recently, our team has proposed two different models for MCFC. The first is a voltage-drop and recovery-analysis model, which can be used to estimate different contributions to transient behavior.[12] The second is a model of current and overpotential distribution, which is based on the analysis of electric conductance of the solution.[13] However, even though much work has been done, a satisfactory numerical analysis method for MCFC is still needed due to extremely complicated physical structures of porous electrodes.

As pointed out by Kazim et al.,[14] in a fuel cell the limiting current density, and thus the maximum power, can often be determined by the maximum species diffusion rate of reactants. Species diffusion limitation depends on the porosity and tortuosity of porous electrodes. Because these systems have intricate dynamical structures, it is necessary to develop powerful numerical methods to treat such problems. In recent years, the lattice Boltzmann method (LBM) has been proposed as an efficient numerical tool to investigate fluid dynamics and various problems with highly complex geometries, such as porous media.[15-19] The LBM allows a detailed discretization of a porous geometry and hence one can have an exact simulation of flows without using any of the semiempirical homogenization approaches. In some sense, the LBM may be considered as a "numerical experiment" with many advantages. For example, it is simple from the viewpoint of arithmetic calculation. It is suitable for large-scale parallel computing, for handling multiphase flow with phase transition, and even for making numerical computations with moving boundaries without loss of computational speed.

It is known that Darcy's flow model combined with the LBM cannot predict correctly reaction-diffusion development in porous media, while the numerical solutions of the Brinkman-Forchheimer-extended Darcy model with LBM were found to compare well with the experimental results for the range of porosity from 0.2 to 0.45 only at low Reynolds numbers, Rayleigh numbers, and Darcy numbers.[15-19] In this work, we shall develop a numerical model for electrochemical kinetics, current density distribution, and species diffusion in MCFC by combining LBM and general principles of the Brinkman-Forchheimer-extended Darcy equations (generalized momentum equation) with the conservation equation of species in porous electrodes. We begin by describing a physical configuration and

[z] E-mail: mmxuys@polyu.edu.hk

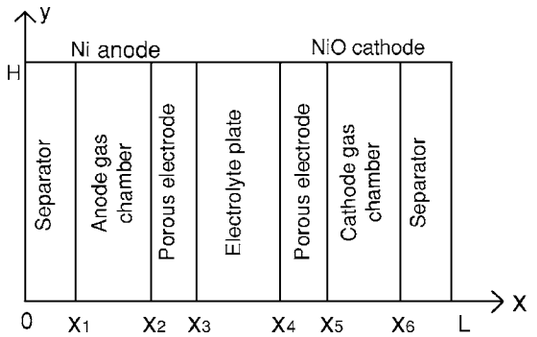

Figure 1. Schematic drawing of the MCFC. See text for explanation.

the Brinkman-Forchheimer-extended Darcy equations together with the reaction-diffusion equation in a porous electrode. Then we extend the LBM model proposed in Refs. 15, 17, and 18 to the MCFC performance. We deal with the scheme for the treatment of boundary conditions, and we give the computational details and validation tests. Some numerical results are also shown. The final section provides a summary of our main results.

The Physical Configuration and Reaction-Diffusion Equation

A porous electrode can be taken as a gas-diffusion electrode due to its large surface area for a charge-transfer reaction within the electrode. To predict its performance and help to optimize its design, much research effort has been devoted to developing an developing an accurate model for porous electrodes.[2] It has been demonstrated that when a MCFC works, O_2 and CO_2 combine at the cathode to form carbonate ions, and anode hydrogen combines with carbonate ions from the cathode to form CO_2 and water. A question of common interest is how an electrochemical process in the fuel cell links with gas-dynamical processes of the transfer of reactant and reaction products in the channel between separator plates and porous electrodes. The dynamics of the oxygen reduction reaction at the porous electrode is associated with physical fuel cell configuration. In the present study, we consider a cross section of the porous electrode, as shown in Fig. 1. It consists of an anode porous electrode, a cathode porous electrode, a separator, and an electrolyte plate. In the figure, L is the length of the fuel cell and H is the height. The subsequent computational domain is therefore the rectangle $(x,y) = (0,L) \times (0,H)$. The primary reaction of the MCFC is similar to other fuel cells. At the anode, H_2 is oxidized electrochemically and CO_2 is generated

$$H_2 + CO_3^{2-} \rightarrow H_2O + CO_2 + 2e \qquad [1]$$

At the cathode, O_2 is electrochemically reduced and CO_2 is consumed

$$\frac{1}{2}O_2 + CO_2 + 2e \rightarrow CO_3^{2-} \qquad [2]$$

The above reaction takes place at the interface between the porous electrode and electrolyte. With the reaction going on, the products accumulate and the reactants reduce. Therefore, gas diffusion takes place in the electrode.

The fuel gas flowing in the porous electrode can be described by a continuity equation and Brinkman-Forchheimer-extended Darcy equations (generalized momentum equation)[20]

$$\nabla \cdot \mathbf{v} = 0 \qquad [3]$$

$$\frac{\partial \mathbf{v}}{\partial t} + (\mathbf{v} \cdot \nabla)\left(\frac{\mathbf{v}}{\phi}\right) = -\frac{1}{\rho}\nabla(\phi P) + \nu_f \nabla^2 \mathbf{v} + \mathbf{F} \qquad [4]$$

where ρ is density, ϕ is porosity, $\mathbf{v}$ is volume-averaged velocity, P is cell total pressure, and ν_f is kinematic viscosity. $\mathbf{F}$ represents total body force due to the presence of the porous medium and other external force fields, expressed by

$$\mathbf{F} = -\frac{\phi\nu}{K}\mathbf{v}_f - \frac{\phi F_\phi}{\sqrt{K}}|\mathbf{v}|\mathbf{v} + \phi G \qquad [5]$$

where G is the body force induced by an external force, and F_ϕ and K are, respectively, the geometric function and permeability, which can be estimated by using Ergun's experimental results[21] and are expressed by[22]

$$F_\phi = \frac{1.75}{\sqrt{150\phi^3}} \qquad [6]$$

$$K = \frac{\phi^3 d_p^2}{150(1-\phi)^2} \qquad [7]$$

where d_p is the effective average diameter of the solid in the porous electrode.

It is known that if concentration is different at different positions, higher concentration gas species will move to lower ones through the electrode that is made of porous media. This process is controlled by the difference in gas concentration, the construction of porous media, and the diffusivity of gas species. For simplicity, we make the following assumptions: (*i*) The flow in the MCFC is considered steady. (*ii*) All changes in the concentration of the carbonate ions are neglected. (*iii*) The concentration of the electrolyte does not change. (*iv*) The system is in a steady state and all changes in the cathode due to corrosion could also be neglected. (*v*) The change of temperature in the cathode can be neglected. Based on these assumptions, the reaction-diffusion equation in the porous electrode can be written as

$$\frac{\partial C_s}{\partial t} + \nabla \cdot (v_s C_s) - D_s \nabla^2 C_s = R_s, \quad 1 \leqslant s \leqslant M \qquad [8]$$

where M is the number of species, v_s is the average velocity of species s, C_s is the mean species concentration of species s at a cross section of the MCFC, R_s is the reaction term depending on C_s and the concentrations of the other species that reacts with s, and D_s is the diffusivity of species s in the porous electrode, given by

$$D_s = D_s' \frac{\phi}{\gamma} \qquad [9]$$

where D_s' is the diffusivity of species s in open void and γ is the tortuosity factor of the electrode. If permeability is in good condition, two kinds of diffusivity are approximately equal. The boundary conditions are then given by

$$C^s(x_2,t) = C^s(x_5,t) = C_0^s, \qquad \left.\frac{\partial C^s(x,t)}{\partial x}\right|_{y=L/2} = 0 \qquad [10]$$

and the initial condition reads

$$C^s(x,t) = C^s(x,t) = 0, \quad x_2 \leqslant x \leqslant x_5 \qquad [11]$$

As reported in Ref. 23, the potential difference caused by different carbonate concentrations at the anode and the cathode can be neglected. Thus the Nernst equation can be written as

$$E_{cell} = E_0 - \frac{RT}{2F_a}\ln[C^{(a)}_{CO_2} C^{(a)}_{H_2O} p^{(a)}] + \frac{RT}{2F_a}\ln[C^{(a)}_{H_2} C^{1/2(c)}_{O_2} C^{(c)}_{CO_2} p^{3/2(c)}] \qquad [12]$$

where E_{cell} is the cell voltage and E_0 is the standard potential and is equal to $1.2723 - 2.7645 \times 10^{-4}T$ for total reaction sum of Eq. 1 and 2, R is the universal gas constant, T is the temperature, and F_a is Faraday's constant. The superscripts (a) and (c) represent, respectively, the anode and cathode, and p is the gas pressure.

Numerical Scheme

Generally, the Boltzmann equation with single-relaxation-time approximation can be written as[24]

$$\frac{\partial f}{\partial t} + \xi \cdot \nabla f = -\frac{1}{\lambda}[f - f^{eq}] \quad [13]$$

where ξ is the particle velocity, f is the particle distribution function, f^{eq} is the equilibrium particle distribution function, and λ is the relaxation time. Discretizing Eq. 13 in the velocity space ξ and using a finite set of discrete velocities $\mathbf{e_i}$, one obtains

$$\frac{\partial f_i}{\partial t} + \mathbf{e}_i \cdot \nabla f_i = -\frac{1}{\lambda}[f_i - f_i^{eq}] \quad [14]$$

In this work, we use the D2Q9 model.[25] The discrete velocities are given by

$$\mathbf{e}_i = \begin{cases} 0 & \text{for } i = 0 \\ \left(\cos\frac{(i-1)\pi}{2}, \sin\frac{(i-1)\pi}{2}\right) & \text{for } i = 1 \sim 4 \\ \sqrt{2}\left(\cos\left[\frac{(i-5)\pi}{2} + \frac{\pi}{4}\right], \sin\left[\frac{(i-5)\pi}{2} + \frac{\pi}{4}\right]\right) & \text{for } i = 5 \sim 8 \end{cases} \quad [15]$$

The local equilibrium distribution function in Eq. 14 can be written as

$$f_i^{eq} = \omega_i \rho\left\{1 + \frac{\mathbf{e}_{i\alpha}\mathbf{v}_\alpha}{c^2} + \frac{\mathbf{v}_\alpha\mathbf{v}_\beta}{2c^2}\left(\frac{\mathbf{e}_{i\alpha}\mathbf{e}_{i\beta}}{c^2} - \delta_{\alpha\beta}\right)\right\} \quad [16]$$

where α and β denote components of Cartesian coordinates (with implied summation for repeated indices), $c = \delta x/\delta t$ is the lattice speed (with δx and δt being lattice distance and time step, respectively), the values of ω_i are given by $\omega_0 = 4/9$, $\omega_i = 1/9$ for $i = 1, 2, 3, 4$, and $\omega_i = 1/36$, for $i = 5, 6, 7, 8$. The density ρ and the velocity $\mathbf{v}$ of the fluid are, respectively, defined by

$$\rho = \sum_i f_i \quad \text{and } \mathbf{v} = \sum_i f_i \mathbf{e}_i/\rho \quad [17]$$

The lattice Boltzmann equation[26] is obtained by further discretizing Eq. 14 in space $\mathbf{x}$ and time t

$$f_i(\mathbf{x} + \mathbf{e}_1\delta t, t + \delta t) - f_i(\mathbf{x}, t) = -\frac{1}{\tau}(f_i - f_i^{eq}) \quad [18]$$

where $\tau = \lambda/\delta t$ is relaxation time. Using a multiscale technique one can recover macroscopic Navier-Stokes equations. In this work, we consider the drag effect of the medium and present the LBM equation by the form of the statistical average

$$\bar{f}_i(\mathbf{x} + \mathbf{e}_i\delta_t, t + \delta_t) = \bar{f}_i(\mathbf{x}, t) - \frac{\bar{f}_i(\mathbf{x}, t) - \bar{f}_i^{eq}(\mathbf{x}, t)}{\tau} + F_i\delta_t \quad [19]$$

where $\bar{f}_i(\mathbf{x}, t)$ and $\bar{f}_i^{eq}(\mathbf{x}, t)$ are volume-averaged distribution function and equilibrium distribution function at representative elementary volume scale, respectively (in the following, the overbars will be omitted for the sake of convenience), F_i is the force term for ith particle of fluid. According to Ref. 27 and 28, F_i is defined as

$$F_i = \omega_i\rho\left(1 - \frac{1}{2\tau}\right)\left(\frac{\mathbf{e}_i \cdot \mathbf{F}}{c^2} + \frac{(\mathbf{e}_i \cdot \mathbf{v})(\mathbf{e}_i \cdot \mathbf{F})}{\phi c^4} - \frac{\mathbf{v} \cdot \mathbf{F}}{\phi c^2}\right) \quad [20]$$

The density and velocity of the fluid are defined by

$$\rho = \sum_i f_i, \quad \mathbf{v} = \sum_i f_i\mathbf{e}_i/\rho + \frac{\delta_t}{2}\mathbf{F} \quad [21]$$

The macroscopic equations for fluid flowing in porous media may be recovered by Taylor expansion and Chapman-Enskog expansion, which read

$$\frac{\partial \rho}{\partial t} + \nabla \cdot (\rho\mathbf{v}) = 0 \quad [22]$$

$$\frac{\partial(\rho\mathbf{v})}{\partial t} + \nabla \cdot \left(\frac{\rho\mathbf{v}\mathbf{v}}{\phi}\right) = -\nabla P + \nabla \cdot [\rho\nu_e(\nabla\mathbf{v} + \mathbf{v}\nabla)] + \mathbf{F} \quad [23]$$

where $\nu_e = (\tau - 0.5)RT\delta_t$. We see that above equations recover Eq. 3 and 4 for ρ = const. Noting that as $\phi = 1$, Eq. 23 is reduced to the standard lattice Boltzmann equation for the fluid flows in the absence of porous media. Another interesting feature of Eq. 23 is that one can get Darcy's law if the flow in porous media is very slow.

To obtain the solution of Eq. 8 for $1 \leqslant s \leqslant M$, we define the total number of particles of species s at time t and position $\mathbf{x}$ as

$$n_s(\mathbf{x}, t) = \sum_i f_s(\mathbf{x}, i, t) \quad [24]$$

It may be related to the mean species concentration C_s of species s in Eq. 8

$$n_s = C_s\frac{(\Delta x)^2}{m_s} \quad [25]$$

where m_s is the unit mass of species s. As usual, we impose the following conditions on f_s^{eq}

$$n_s(\mathbf{x}, t) = \sum_i f_s(\mathbf{x}, i, t) = \sum_i f_s^{eq}(\mathbf{x}, i, t) \quad [26]$$

$$n_s\mathbf{v}_s(\mathbf{x}, t) = \sum_i \mathbf{e}_1 f_s^{eq}(\mathbf{x}, i, t) \quad [27]$$

where $\mathbf{v}_s(\mathbf{x}, t)$ is the local velocity of species s. Equation 27 represents the conservation of local mass for a nonreactive system. For a MCFC system, one can select the following simple equilibrium distribution function

$$f_s^{eq}(\mathbf{x}, i, t) = \frac{n_s}{n_0} f_0^{eq}(\mathbf{x}, i, t) \quad [28]$$

where subscript 0 refers to the solvent, and $f_0^{eq}(\mathbf{x}, i, t)$ is the same as in Ref. 17. Using a multiscale technique we recover the following reaction-diffusion equation

$$\frac{\partial C_s}{\partial t} + \nabla \cdot (C_s\mathbf{v}) - \kappa_s^2(\tau_s - 0.5)\nabla^2 C_s = R_s \quad [29]$$

where κ_s is sound velocity, C_s is the concentration of the species s, and R_s is the reaction rate for species s as in Eq. 3. The diffusivity of species s is given by

$$D_s = \kappa_s^2(\tau_s - 0.5) \quad [30]$$

Analysis of Boundary Conditions

It is well known that, in the simulation of diffusion in a MCFC, boundary conditions are extremely important for obtaining accurate results. Bouncing-back boundary condition[29] is a primary method in the lattice-Boltzmann simulation and has been proved to have a first-order accuracy. To increase accuracy, more accurate boundary conditions have been proposed in the past few years.[30-33] In this study, a curved boundary lying between the nodes of the equidistant lattice space $\Delta\delta x$ for a 2D model is proposed, which has been shown in Fig. 2.

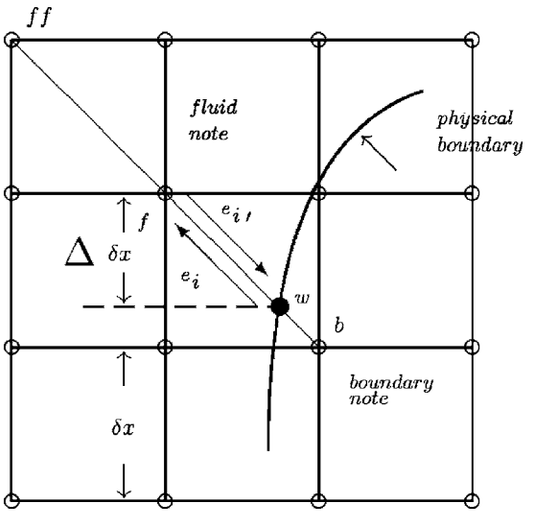

Figure 2. Layout of regularly spaced lattice and curved wall boundary for a porous electrode in the MCFC.

To proceed, we take $\mathbf{x}_b$ and $\mathbf{x}_f$ to denote, respectively, the lattice node for the solid side and fuel fluids side of the porous electrode. Let $\mathbf{e}_i = \mathbf{x}_b - \mathbf{x}_f$ and $\mathbf{e}_{i'} = -\mathbf{e}_i$ and assume the filled small circle at $\mathbf{x}_w$ is the intersection with the physical boundary on the link between $\mathbf{x}_b$ and $\mathbf{x}_f$. The fraction of an intersected link in the fuel fluid is Θ, defined by

$$\Theta = \frac{|\mathbf{x}_f - \mathbf{x}_w|}{|\mathbf{x}_f - \mathbf{x}_b|}, \quad 0 \leqslant \Theta \leqslant 1 \qquad [31]$$

After a collision step, the distribution function at $\mathbf{x}_f$ and t is given by the following streaming step

$$f_i(\mathbf{x}_f, t + \delta t) = f_i(\mathbf{x}_{ff}, t) \qquad [32]$$

while $f_{i'}(\mathbf{x}_f)$ can be obtained by

$$f_{i'}(\mathbf{x}_f, t + \delta t) = f_{i'}(\mathbf{x}_b, t) \qquad [33]$$

However, the distribution function $f_{i'}(\mathbf{x}_b, t)$ at boundary node is unknown. According to Ref. 24, we assume that $f_{i'}(\mathbf{x}_b, t)$ satisfies the following linear interpolation formula

$$f_{i'}(\mathbf{x}_b, t) = (1 - \chi) f_i(\mathbf{x}_f, t) + \chi f_i^*(\mathbf{x}_b, t) + 6\alpha_i \mathbf{e}_{i'} \cdot \mathbf{v}_w \qquad [34]$$

where $\mathbf{v}_w = \mathbf{v}(\mathbf{v}_w, t)$ is the velocity at the physical boundary and χ is a parameter. f_i^* is a fictitious equilibrium distribution function, given by

$$f_i^*(\mathbf{x}_b, t) = \omega_i \rho \left\{ 1 + \mathbf{e}_{i\alpha} \cdot \mathbf{v}_{\alpha bf} + \frac{\mathbf{v}_{\alpha f} \cdot \mathbf{v}_{\beta f}}{2} (\mathbf{e}_{i\alpha} \cdot \mathbf{e}_{i\beta} - \delta_{\alpha\beta}) \right\} \qquad [35]$$

where $\mathbf{v}_{\alpha f} = \mathbf{v}_\alpha(\mathbf{x}_b, t)$ and $\mathbf{v}_{\beta f} = \mathbf{v}_\beta(\mathbf{x}_b, t)$ are the fluid velocity near the solid and $\mathbf{v}_{bf}$. $\mathbf{v}_{bf}$ can be chosen as[32]

$$\mathbf{v}_{bf} = (\Theta - 1)\mathbf{v}_f/\Theta + \mathbf{v}_w/\Theta \quad \text{and } \chi = (2\Theta - 1)/\tau \quad \text{for } \Theta \geqslant \frac{1}{2} \qquad [36]$$

and

$$\mathbf{v}_{bf} = \mathbf{v}_f \quad \text{and } \chi = (2\Theta - 1)/(\tau - 1) \quad \text{for } \Theta \leqslant \frac{1}{2} \qquad [37]$$

To improve the stability of the scheme, Eq. 31 can be replaced by[34]

$$\mathbf{v}_{bf} = \mathbf{v}_{ff} \quad \text{and } \chi = (2\Theta - 1)/(\tau - 2) \quad \text{for } \Theta \leqslant \frac{1}{2} \qquad [38]$$

The boundary conditions for species concentration can be implemented in the following way.[35] If the concentration on the boundary node $\mathbf{x}_b$ is known, the concentration distribution function can be calculated by

$$C_i(\mathbf{x}_b) - C_i^{eq}(\mathbf{x}_b) = C_i(\mathbf{x}_f) - C_i^{eq}(\mathbf{x}_f) \qquad [39]$$

where $C_i^{eq}(\mathbf{x}_b)$ is obtained from Eq. 28. Meanwhile, if we know the concentration gradient on the boundary node $\mathbf{x}_b$, we can calculate the concentration distribution function via the formula

$$C_i(\mathbf{x}_b) = \omega_i [C_i(\mathbf{x}_f) - (\mathbf{x}_f - \mathbf{x}_b) \cdot \nabla C_i(\mathbf{x}_b)] \left[\sigma + \frac{\mathbf{e}_i \cdot \mathbf{v}(\mathbf{x}_b)}{c^2} \right] + C_i(\mathbf{x}_f, t) - C_i^{eq}(\mathbf{x}_f) \qquad [40]$$

Computational Results and Discussion

Comparison between simulation and analytical analysis.— In a MCFC, the main properties of interest are the cell voltage, current density, power density, removal of the CO_2, and the contribution of CO_2 concentration on cell performance under different applied loads. In our simulation, we suppose that the resistance in the current collectors is negligible in order to avoid that the numerical result might be different from the experimental values. Cell voltage can be calculated from Eq. 12. With equilibrium potentials in the cathode, $E_{eq,c}$, and the anode, $E_{eq,a}$, the potential drop in the cathode, electrolyte matrix, and the anode can be calculated. Overall potential drop can be determined by the deviation of the cell voltage from equilibrium potential ($E_{eq} - E_{cell}$).

To validate the numerical solution, necessary physical parameters and data are needed. Some of them can be found in Ref. 8, but others are necessary to be measured experimentally. In Table I we have listed all these parameters and some data we measured experimentally. Note that the numerical solution should validate against the analytical solution by Anisin et al.[36] where a theoretical model for MCFC was developed based on variable gas mixture composition, with inclusion of reactants and electrochemical reaction products between the separator plate and the anode. Their analytical solution reads

$$C(x,y) = C_0 = \frac{4c_0}{\pi} \sum_{n=0}^{\infty} (-1)^n \frac{\cos \dfrac{(2n+1)\pi y}{2L}}{2n+1} \exp\left[-\frac{\pi^2 D x}{4L^2 v} (2n+1)^2 \right] \qquad [41]$$

where C_0 is a constant. Relation 41 determines a stationary distribution of gas concentration at any channel point in the absence of

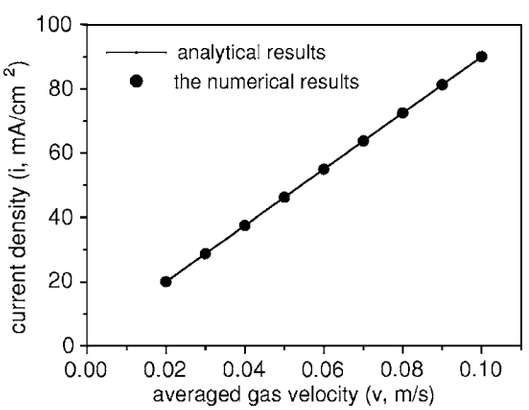

Figure 3. Comparison of the dependence of generated current density on averaged gas velocity between the LBM result (solid circles) and the theoretical solution using Eq. 41 (solid line).

Table I. Parameters of the MCFC used in model simulation.

Parameter	Value	Reference
Diffusion coefficient of CO_2 in the liquid phase in cathode, $D^{l}_{CO_2,c}$	$1e^{-3}$ cm^2/s	8
Diffusion coefficient of O_2 in the liquid phase in cathode, $D^{l}_{O_2,c}$	$3e^{-3}$ cm^2/s	8
Diffusion coefficient of CO_2 in the gas phase in cathode, $D^{l}_{CO_2,c}$	1.16 cm^2/s	8
Diffusion coefficient of O_2 in the gas phase in cathode, $D^{l}_{O_2,c}$	1.16 cm^2/s	8
Diffusion coefficient of CO_2 in the liquid phase in anode, $D^{l}_{CO_2,a}$	1.0 cm^2/s	8
Diffusion coefficient of H_2 in the gas phase in anode, $D^{l}_{H_2,a}$	1.0 cm^2/s	8
Diffusion coefficient of CO_2 in the gas phase in anode, $D^{l}_{CO_2,a}$	4.625 cm^2/s	8
Diffusion coefficient of O_2 in the gas phase in anode, $D^{l}_{O_2,a}$	4.625 cm^2/s	8
Cathode conductivity, σ_c	13.0 S/cm	8
Electrode conductivity, κ	2.0×10^2 S/cm	8
Length of fuel cell, L	0.52 cm	Measured
Thickness of the anode, $x_3 - x_2$	0.1 cm	Measured
Thickness of the cathode, $x_5 - x_4$	0.1 cm	Measured
Thickness of the matrix, $x_4 - x_3$	0.12 cm	Measured
Liquid porosity in the cathode, ϕ^l_c	0.31	Measured
Gas porosity in the cathode, ϕ^g_c	0.39	Measured
Solid porosity in the cathode, ϕ^s_c	0.31	Measured
Liquid porosity in the anode, ϕ^l_a	0.22	Measured
Gas porosity in the anode, ϕ^g_a	0.38	Measured
Solid porosity in the anode, ϕ^s_a	0.33	Measured
Liquid porosity in the electrolyte matrix, ϕ^l_e	0.7	Measured
Equilibrium potential of the cathodic reaction, $E_{eq,c}$	0 V	8
Equilibrium potential of the anodic reaction, $E_{eq,a}$	−1.02 V	8
Rate constant of the molar flux of CO_2 between the liquid and gas phase in the cathode, $k^{lg}_{CO_2,c}$	3×10^3 cm/s	8
Rate constant of the molar flux of O_2 between the liquid and gas phase in the cathode, $k^{lg}_{O_2,c}$	2×10^3 cm/s	8
Rate constant of the molar flux of CO_2 between the liquid and gas phase in the anode, $k^{lg}_{CO_2,a}$	3×10^3 cm/s	8
Rate constant of the molar flux of H_2 between the liquid and gas phase in the cathode, $k^{lg}_{H_2,a}$	2×10^3 cm/s	8
Cathodic transfer coefficient in the cathode, $\alpha_{c,c}$	0.5	8
Anodic transfer coefficient in the cathode, $\alpha_{a,c}$	1.5	8
Cathodic transfer coefficient in the anode, $\alpha_{c,a}$	1.5	8
Anodic transfer coefficient in the anode, $\alpha_{a,a}$	0.5	8
Cell temperature, T	650°C	Measured

gas friction at the separator walls and gas diffusion into separator walls, with the gas moving along the channel at average speed v. Our numerical simulation based on the LBM is performed with a lattice size of 50×256. In Fig. 3 we present the numerical result (solid circles) and make a comparison of the dependence of the generated current density on averaged gas velocity between the LBM result and the analytical solution using Eq. 41 (solid line). We see that the LBM result agrees well with that obtained by the analytical solution. To further validate our LBM model, we have measured the current density experimentally in an available range of H_2 concentration and made a careful comparison between the experimental result and the one by using the LBM model, which has been shown in Fig. 4. In the figure, the triangles and squares are two groups of experimental data and the solid circles represents the re-

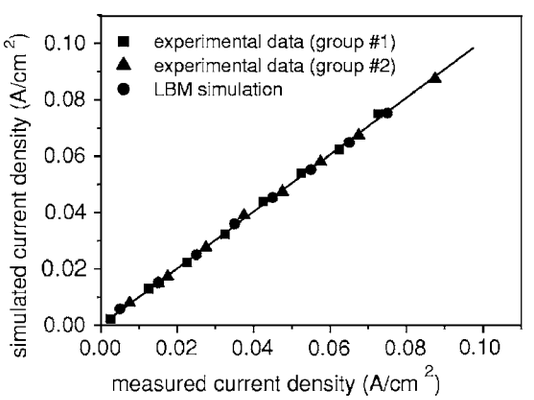

Figure 4. Comparison of current density between the result by simulation (solid circles) and the ones through experimental measurement (solid triangles and solid squares) in the overall experimental range of H_2 concentration.

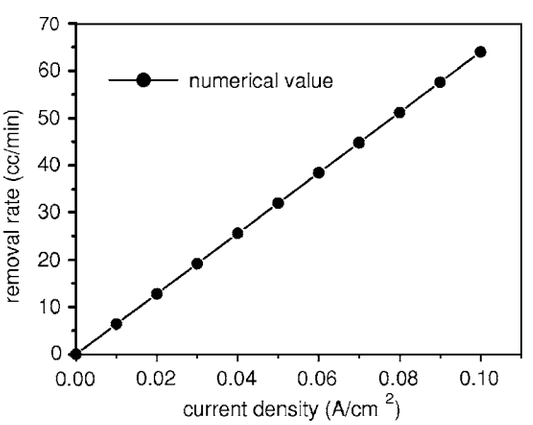

Figure 5. The dependence of CO_2 removal rate on current density.

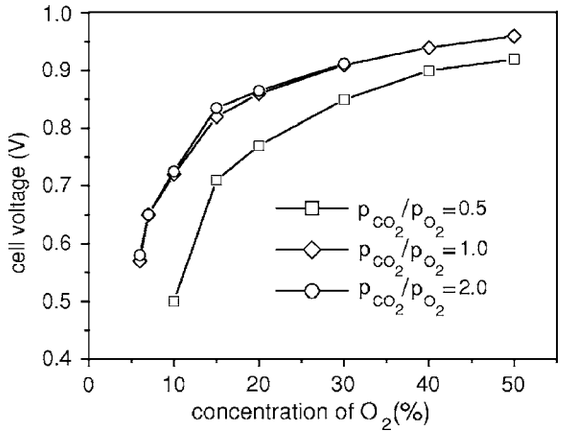

Figure 6. Effect of CO_2 concentration on cell performance.

sult obtained through the LBM simulation. In our experiment, data are collected on a sample of fuel cells, tests are performed at 650 K, temperature keeps constant on the cell plane using heating plate, and other operating conditions in the simulation are the same as those of the measurement in Ref. 37. We see that there is an excellent agreement between the LBM simulation and the experimental measurement.

In the MCFC, the removal of CO_2 is very important. Generally, the CO_2 removal rate Q_{CO_2} is evaluated by measuring the flow rate of cathode exhaust gas with each current density, which is defined by[38]

$$Q_{CO_2} = 0.667(V_{OCV} - V_1) \quad [42]$$

where V_{OCV} means flow rate of cathode exhaust gas at open-circuit-voltage and V_1 is the flow rate of cathode exhaust gas at on-load. Figure 5 shows the dependence of CO_2 removal rate on current density when fuel gas utilization is 75% and oxidant gas utilization is 50%. The removal rate increases with increasing current density, indicating a strong dependence of CO_2 removal rate on the current density.

Effect of CO_2 *and* O_2 *concentration on cell performance.*— To understand further the effect of CO_2 and O_2, we have made simulations on the cell performance against different gas concentrations. The results are presented in Fig. 6 and Fig. 7. The parameters used in the simulations are tabulated in Table II. Figure 6 shows the influence of CO_2 concentration on cell voltage. One sees that a sharp decrease occurs when the CO_2 concentration is 10% or less.

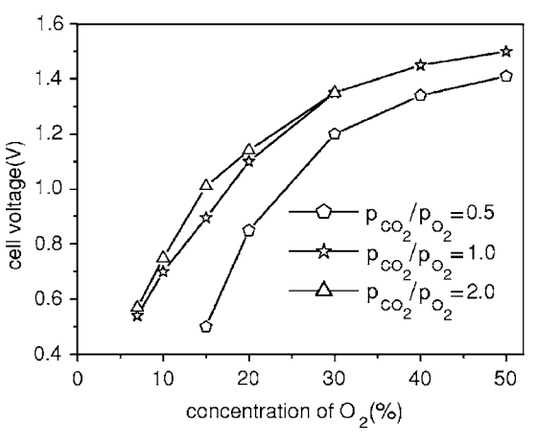

Figure 7. Effect of O_2 concentration on cell performance.

Table II. Parameters used in the analysis on the effects of CO_2 concentration and O_2 concentration on the cell performance.

Current density (mA/cm^2)	Partial pressure ratio (p_{CO_2}/p_{O_2})	Fuel gas utilization (%)	CO_2 gas utilization (%)	Oxidant gas utilization (%)
100	0.5, 1.0, 2.0	45	50	40

Figure 7 shows that the cell voltage decreases as O_2 concentration is lowered, and there is also a sharp decrease when the O_2 concentration becomes nearly 30%. From the results given by Fig. 6 and Fig. 7, we see that the O_2 species is a dominant factor for the cell performance, consistent with the result by Uchida's group.[39-41] In addition, the cell voltage can be improved by decreasing the partial pressure ratio.

Finally, the results of the cell voltage and the power density as functions of the current density are illustrated in Fig. 8. We see that the cell voltage drops almost linearly with the increasing of applied current density. This was observed both in our simulations and the experimental measurement. Such behavior is expected because the activation polarization, observed in the low-temperature fuel cell at low current density, vanishes in a high-temperature cell.[8] Power density is defined as the product of the applied current density and the voltage. One sees from the figure that the power density curve against current density is a quasi-parabolic one, which increases initially with the current density, reaches a peak, and then decreases. The maximum power density is about 180 mW/cm^2 at the current density around 350 mA/cm^2.

Conclusions

In this work, a LBM model is proposed to simulate MCFC performance. Detail computational results have been provided, which lead to the following conclusions.

1. The result of a simulation on the dependence of the generated current density on averaged gas velocity agrees well with that obtained by an analytical analysis.
2. To test the simulating result on the current density, related experimental measurement has been conducted. A quite good agreement between the experimental result and the computational one is found in the overall experimental range of H_2 concentration.
3. The result of the dependence of CO_2 removal rate on current density reveals that the stronger the current density, the higher the removal rate, indicating the amount of CO_2, which moves from the cathode to the anode, is an important factor for the cell performance.
4. It is found that the cell voltage decreases as CO_2 concentration and O_2 concentration are lowered, while the O_2 species is a dominant factor for the cell performance.

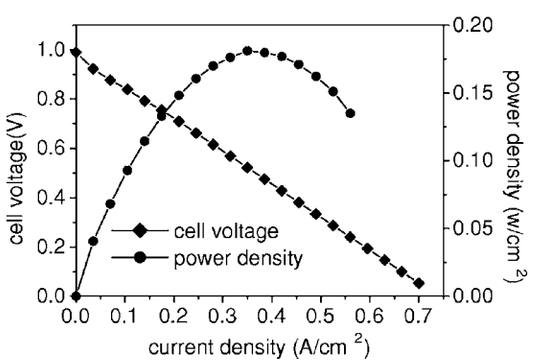

Figure 8. The functional relations of cell voltage and power density with current density (load).

5. In the MCFC, the cell voltage drops almost linearly with the increase of applied current density. This has been observed both in the model simulation and the experimental measurement. The power-density curve displays a parabolic behavior, i.e., as current density increases, it increases initially, reaches a peak value, and then decreases.

Acknowledgments

This work was supported by the National Natural Science Foundation of China under grants no. 10572130, 90403008, and 10434060, by the State Key Development Program for Basic Research of China under grant no. 2005CB724508, and by the Research Grants Council of the Government of the HKSAR under grant no. PolyU5172/02.

East China Normal University assisted in meeting the publication costs of this article.

References

1. C. Y. Yuh and J. R. Selman, *J. Electrochem. Soc.*, **139**, 1373 (1992).
2. S. G. Hong, J. R. Selman, and C. Y. Yuh, *J. Electrochem. Soc.*, **151**, A748 (2004).
3. G. Wilemki, *J. Electrochem. Soc.*, **130**, 117 (1983).
4. C. Y. Yuh and J. R. Selman, *J. Electrochem. Soc.*, **131**, 2062 (1984).
5. E. Fontes, M. Fontes, and D. Simonsson, *Electrochim. Acta*, **40**, 1641 (1995).
6. E. Fontes, C. Lagergren, and D. Simonsson, *J. Electroanal. Chem.*, **432**, 121 (1997).
7. J. D. Fehribach et al., *J. Appl. Electrochem.*, **30**, 1015 (2000).
8. N. Subramainian et al., *J. Electrochem. Soc.*, **150**, A1360 (2003).
9. M. Mangold and M. Sheng, *Fuel Cells*, **4**, 68 (2004).
10. M. Fermeglia et al., *Fuel Cells*, **5**, 66 (2004).
11. F. Yoshiba, *Int. J. Energy Res.*, **28**, 1361 (2004).
12. X. Z. Xu, K. Tanimoto, and S. Kimihiko, *J. Electrochem. Soc.*, **149**, 1 (2002).
13. M. Zhu, X. Z. Xu, R. Su, and J. M. Yang, *J. Electrochem. Soc.*, **152**, A511 (2005).
14. A. Kazim, H. T. Liu, and P. Forges, *J. Appl. Electrochem.*, **29**, 1409 (1999).
15. Z. L. Guo and T. S. Zhao, *Phys. Rev. E*, **66**, 036304 (2002).
16. Q. Kang, D. Zhang, S. Y. Chen, and X. He, *Phys. Rev. E*, **65**, 036318 (2002).
17. S. P. Dawson, S. Chen, and G. D. Doolen, *J. Chem. Phys.*, **98**, 1514 (1992).
18. R. Kumar et al., *Int. J. Numer. Methods Fluids*, **31**, 801 (1999).
19. Y. S. Xu, Y. Liu, and G. X. Huang, *Chin. Phys. Lett.*, **21**, 2454 (2004).
20. P. Nithiarasu, K. N. Seetharamu, and T. Sundararajan, *Int. J. Heat Mass Transfer*, **40**, 3955 (1997).
21. S. Ergun, *Chem. Eng. Prog.*, **48**, 89 (1952).
22. K. Vafai, *J. Fluid Mech.*, **147**, 233 (1984).
23. D. Gidaspow, in *Porous Electrodes, Theory and Practice*, Hans C. Maru, T. Katan, and M. G. Klein Editors, PV 84-8, p. 350, The Electrochemical Society Proceedings Series, Pennington, NJ (1984).
24. P. L. Bhatnagar, E. P. Gross, and M. Krook, *Phys. Rev.*, **94**, 511 (1954).
25. Y. H. Qian, D. d'Humiéres, and P. Lallemand, *Europhys. Lett.*, **17**, 479 (1992).
26. H. Chen, S. Chen, and W. H. Matthaeus, *Phys. Rev. A* **45**, R5339 (1992).
27. A. Cancelliere et al., *Phys. Fluids A*, **2**, 2085 (1990).
28. K. J. Maloy et al., *Phys. Rev. Lett.*, **68**, 2161 (1992).
29. D. R. Noble et al., *Phys. Fluids*, **7**, 203 (1995).
30. H. P. Fang, Z. F. Lin, and Z. W. Wang, *Phys. Rev. E*, **57**, R25 (1998).
31. X. He, Q. Zou, and M. Dembo, *J. Stat. Phys.*, **87**, 115 (1997).
32. Q. Filippova and D. Hanel, *Comput. Fluids*, **26**, 697 (1997).
33. Z. Guo, C. Zheng, and B. Shi, *Phys. Fluids*, **14**, 2007 (2002).
34. R. W. Mei, L. S. Luo, and W. Shyy, *J. Comput. Phys.*, **155**, 307 (1999).
35. Z. Guo and T. S. Zhao, *Numer. Heat Transfer, Part B*, **47**, 1 (2004).
36. A. V. Anisin, I. A. Davydov, and A. V. Kondrashenko, *Russ. J. Electrochem.*, **39**, 898 (2003).
37. E. Arato et al., *J. Power Sources*, **102**, 74 (2001).
38. K. Sugiura et al., *J. Power Sources*, **118**, 218 (2003).
39. K. Yamada, T. Nishina, I. Uchida, and J. R. Selman, *Electrochim. Acta*, **38**, 2045 (1993).
40. K. Yamada, T. Nishina, and I. Uchida, *Electrochim. Acta*, **40**, 1927 (1995).
41. T. Itoh et al., *J. Electrochem. Soc.*, **151**, A2042 (2004).